IOP Conference Series: Materials Science and Engineering

PAPER • **OPEN ACCESS**

Experimental Characterisation and Numerical Modelling of the Effect of Cold Rolling on the Nanoindentation Response of Pure Zinc Grains

To cite this article: P T N Nguyen *et al* 2019 *IOP Conf. Ser.: Mater. Sci. Eng.* **540** 012011

View the article online for updates and enhancements.

IOP ebooks™

Bringing you innovative digital publishing with leading voices to create your essential collection of books in STEM research.

Start exploring the collection - download the first chapter of every title for free.

This content was downloaded from IP address 123.134.247.94 on 18/09/2019 at 22:31

IOP Conf. Series: Materials Science and Engineering **540** (2019) 012011 doi:10.1088/1757-899X/540/1/012011

Experimental Characterisation and Numerical Modelling of the Effect of Cold Rolling on the Nanoindentation Response of Pure Zinc Grains

P T N Nguyen[1,2], F Abbès[2], B Abbès[2], J-S Lecomte[3] and C Schuman[3]

1 The University of Danang, University of Science and Technology, Da Nang, Vietnam
2 GRESPI, University of Reims Champagne-Ardenne, France
3 LEM3, University of Lorraine, Metz, France
E-mail: fazilay.abbes@univ-reims.fr

Abstract. In this study, the orientation-dependent response of as-received annealed cold-rolled pure zinc and material with thickness reduction rate of 50% grains using instrumented indentation tests is investigated. The experiments were characterized by orientation microscopy and atomic force microscopy scans to quantify the orientation-dependent mechanical response during nanoindentation. The single crystal hardening parameters are then identified for each family of slip system by using crystal plasticity finite element (CPFE) simulations. Comparison between experimental and numerical results in terms of "load-penetration depth" curves show a good agreement. The increased percentage of cold reduction increases the identified critical resolved shear stress (CRSS). Finally, the accuracy of the model is evaluated by comparing experimental and numerical data issued from nanoindentation response grains of distinct crystalline orientations involving different slip systems activity rates.

1. Introduction

Zinc is well-suited for corrosion protective coating for iron and steel products. It is successfully used as a protective coating on a variety of products and in many exposure conditions, especially in automotive applications (hot-dip galvanized sheets) for its high corrosion resistance in most environments. An efficient coating requires a good forming ability and adhesive bonding, with no crack or flaking during forming process. Zinc has a hexagonal close-packed (HCP) crystalline structure. Zinc is characterized by a high lattice ratio exhibiting a strong anisotropic behaviour compared to other HCP metals like titanium or magnesium $\left(\frac{c}{a}\Big|_{Zn}=1.856,\ \frac{c}{a}\Big|_{Mg}=1.624,\ \frac{c}{a}\Big|_{Ti}=1.588\right)$.

HCP sheet forming finite element simulations have been generally performed using classical macroscopic anisotropic criteria [1, 2]. A physically based approach requires a good understanding of the deformation mechanisms: dislocation slip at the individual grain scale in the polycrystalline sample. Moreover, the grain response involves different slip systems activity rates depending on its orientation. Recent advances in the developing of macroscopic plasticity models for HCP materials have allowed a better capture of specific features like the anisotropy and the tension-compression asymmetry in yielding of HCP metals [3-8]. An accurate determination of slip resistance and its evolution is of very importance to well predicting the macroscopic response of a polycrystalline material. In practice, instrumented indentation tests performed on grains of distinct crystallographic orientations allows determining indirectly the critical resolved shear stresses (CRSS) of all systems.

Content from this work may be used under the terms of the Creative Commons Attribution 3.0 licence. Any further distribution of this work must maintain attribution to the author(s) and the title of the work, journal citation and DOI.
Published under licence by IOP Publishing Ltd

To achieve this, an inverse parameter identification procedure combining crystal plasticity finite element method (CPFEM) with an optimization algorithm is needed [9-11]. In this study, material parameters were determined by inverse method: finite element simulations of the nanoindentation tests are used, and the parameters are varied systematically until agreement between simulations and experiments is achieved. The objective function is the deviation between experimental and numerical results in terms of "load-penetration depth" curves issued from the nanoindentation experiments performed on grains of given crystalline orientation. Cold-rolled grains of pure polycrystalline zinc sheets are considered. The identified CPFEM parameters for materials with different reduction rates are compared.

2. Crystal Plasticity model

In the crystal plasticity theory, the plastic deformation results from the cumulative effect of crystalline glide in all activated slip systems. The deformation rate is the sum over all the shear rates contributed by all activated systems. The shear strain rate $\dot{\gamma}^{(\alpha)}$ on the α^{th} slip system obeys Schmid's law and is given by the following power-law:

$$\dot{\gamma}^{(\alpha)} = \dot{\gamma}_0{}^{(\alpha)} \left| \frac{\tau^{(\alpha)}}{\tau_c{}^{(\alpha)}} \right|^n sgn\left(\tau^{(\alpha)}\right) \tag{1}$$

where $\dot{\gamma}_0{}^{(\alpha)}$ is the reference shear strain rate on slip system α, $\tau^{(\alpha)}$ is the resolved shear stress, $\tau_c{}^{(\alpha)}$ is the slip resistance or critical resolved shear stress of the slip system α, and n is the strain-rate sensitivity exponent.

For multiple slip, the evolution of the slip resistance $g^{(\alpha)}$ is governed by the hardening law expressed as:

$$\dot{g}^{(\alpha)} = \sum_{\beta} h_{\alpha\beta} \dot{\gamma}^{\beta} \tag{2}$$

where $h_{\alpha\beta}$ are the slip hardening moduli, the sum ranges over all activated slip systems. $h_{\alpha\alpha}$ and $h_{\alpha\beta}$ ($\alpha \neq \beta$) are the self and latent hardening moduli, respectively.

Peirce *et al.* [12] have expressed the relation between self and latent hardening moduli as follows:

$$\begin{cases} h_{\alpha\alpha} = h(\gamma) = h_0 \sec h^2 \left| \dfrac{h_0 \gamma}{\tau_s - \tau_0} \right| \\ h_{\alpha\beta} = q h(\gamma) \quad (\alpha \neq \beta) \end{cases} \tag{3}$$

where h_0 is the initial hardening modulus, τ_0 is the critical resolved shear stress and τ_s is the saturation strength. γ is the Taylor cumulative shear strain on all slip systems defined as:

$$\gamma = \sum_{\alpha} \int_0^t \left| \dot{\gamma}^{(\alpha)} \right| dt \tag{4}$$

The parameter q is defined as the ratio of latent over self-hardening moduli and characterizes the hardening behaviour. It, taken equal to unity in our simulations.

The basal glide ($B\langle a\rangle\{0001\}\langle 11\bar{2}0\rangle$) is the primary slip system for zinc because of its high lattice ratio. The overall deformation is accommodated by prismatic glide ($P\langle a\rangle\{10\bar{1}0\}\langle 11\bar{2}0\rangle$) and second-order pyramidal glide ($\Pi_2\langle c+a\rangle\{11\bar{2}2\}\langle 11\bar{2}3\rangle$) to satisfy the Taylor criterion [13] requiring five independent slip systems for the ductility of polycrystalline metals. It is worth mentioning that we have not considered first-order pyramidal slip systems ($\Pi_1\langle a\rangle$). Indeed, the analysis of Yoo and Wei [14] showed that basal and prismatic slip systems are cristallographically equivalent to $\Pi_1\langle a\rangle$ glide. Following the work of Yoo and Lee [15], zinc exhibits compression twinning $\{10\bar{1}2\}\langle 10\bar{1}\bar{1}\rangle$ causing a

contraction along the c-axis. However, no twinning was observed in the nanoindentation experiments we have carried out, therefore the compression twin system is not considered in this study.
The crystal plasticity model for an HCP crystal was implemented into the implicit finite element (FE) code ABAQUS/Standard through a user material subroutine (UMAT), initially developed by Huang [16] for cubic system and modified by Kysar and Hall [17]. In the FE formulation, the plastic deformation is assumed due solely to the crystallographic dislocation glide. The deformation by diffusion, twinning and grain boundary sliding is not considered here.

3. Instrumented indentation tests

The first studied material is the as-received annealed cold-rolled sheet (1 mm thickness) of high-purity polycrystalline zinc (Zn > 99.99 + wt%) named "AR". The chemical composition is given in table 1. The second studied material is the as-received sheets that have been plastically deformed (thickness reduction rate of 50%) named "TR" and annealed at a temperature of 100°C for a period of 2 h to trigger the recrystallization of new grains.

Table 1. Chemical analysis (ppm) of as-cast high purity (99.99+ %) polycrystalline zinc.

Ag	Cd	Ca	Cr	Cu	Cs	Fe	Mn	Ni	Pd	Pb	Rh	Ta	T	Ti
0.36	3.4	<0.1	0.55	4.0	<0.1	4.9	0.18	0.66	<1	12	<0.5	<10	5.1	4.5

Microstructure characterization was evaluated by electron backscatter diffraction (EBSD) using a JEOL65 field emission gun-scanning (FEG) electron microscope (SEM) equipped with OIM EBSD system. Samples preparations for EBSD examination were first ground with sand paper, and then were polished with 1µm diamond paste to mirror finish. In order to achieve the surface quality required for nanoindentation tests and EBSD examination (*i.e.* deformation-free and scratch-free surface) a chemo-mechanical polishing with colloidal silica suspension (~ 40nm) on porous neoprene polishing cloth for about 35nm was used.
Instrumented indentation tests were performed using a 90° cono-spherical diamond indenter (tip radius of 1 µm) mounted in a NHT-2 nanoindenter (CSM Instruments). Indentations were carried out in load-control mode.
The selected grains for nanoindentation tests are located in the standard stereographic triangle as shown in figure 1. The crystalline orientation using the Euler-Bunge angles of those grains are listed in table 2. The grains for which the <c> axis (*i.e.* <0001>) is parallel to the normal direction of the sheet are called basal grains. Grains for which the $\langle \bar{1}2\bar{1}0 \rangle$ direction is parallel to the normal direction of the sheet are called pyramidal grains. Finally, grains for which the $\langle 01\bar{1}0 \rangle$ direction is along the normal direction of the sheet are called prismatic grains. To avoid grain boundary influence, indents were located in the mid-zone of individual grains.

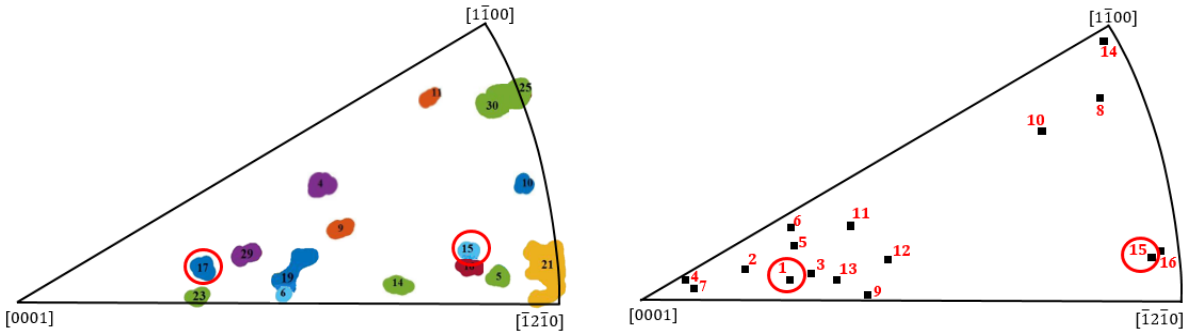

Figure 1. Location of the selected grains: AR (Left) – TR (Right).

Table 2. Crystalline orientation of the selected grains.

Grain number	Crystalline orientation	State	Euler-Bunge angle (°)		
			φ_1	ϕ	φ_2
1	Basal	TR	2.4	23.3	37.6
15	Pyramidal	TR	50.3	83.8	24.7
17	Basal	AR	114.9	28.4	189.8
15	Pyramidal	AR	69.6	107.1	186.3

4. Identification process

Three-dimensional finite element simulations of the nanoindentation tests were performed using the commercial software ABAQUS. Assuming a single-crystal-like behaviour, the grain has been modelled as a cylinder of 20 µm diameter and 20 µm height. The sample was discretized using 13860 eight-node linear hexahedral elements with reduced integration scheme (C3D8R), and the mesh size with the smallest element size equals to 60 nm to ensure that the mesh was fine enough near the area in contact with the indenter. To keep the simulations computationally tractable, the mesh density was progressively coarsened away from the grain center. To avoid grain-boundary effects, the bottom and surrounding surfaces the specimen were constrained. The indenter was only allowed to move in the z direction. The FE mesh is illustrated in figure 2.

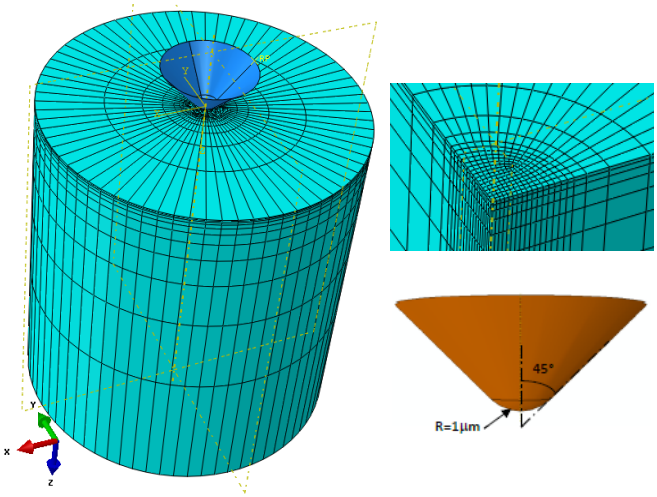

Figure 2. Three-dimensional Finite element mesh.

To investigate the sensitivity and confirm the convergence of the proposed mesh size on the numerical simulation, we have used the model of 13860 elements and the mesh size with the smallest element size of 60 nm as a benchmark. Three modified cases of mesh size were considered, namely: 10% smaller, 10% larger, and 30%. The obtained results showed that for the case with 30% larger element size (the smallest element size is 78 nm), the deviation of the penetration depth and the pile-up height from the benchmark was 5.2%. For the case with 10% larger element size, the deviation was 4.1% and for the case with 10% smaller size (the smallest element size is 54 nm) the deviation was only 0.4%. Based on this sensitivity analysis the selected model with 13860 elements is enough to get the converging solution.

The cono-spherical indenter was modelled as a fully rigid body, with a tip radius of 1 µm and a half included angle of 45 °. A friction coefficient of 0.1 was assumed between the indenter and the zinc substrate. Even if friction is known to play a minor role on the load vs. displacement response during

indentation [18-19], the use of a friction coefficient enhances convergence by limiting mesh elements distortion in the contact area.
Furthermore, like experimental conditions, all simulations were performed under quasi-static, isothermal load-controlled conditions. In addition, nonlinearity option was used to account for both material and geometric (finite strains and rotations) nonlinearities.
The stiffness tensor **C** was considered to model the single crystal elastic response, which is composed with the six following terms: C_{11}= C_{22}= 165 GPa, C_{12}= 31.1 GPa, C_{13}= C_{23}= 50 GPa, C_{33}= 61.8 GPa, C_{44}= C_{55}= 39.6 GPa, C_{66}= 66.95 GPa.
Since plastic deformation is obtained by crystallographic dislocation slips, a total of 12 slip systems was considered: basal slip systems (3), prismatic slip systems (3) and Π_2 $\langle c+a \rangle$ slip systems. According to the proposed crystal plasticity model, four material parameters ($h_0^{(\alpha)}$, $\tau_0^{(\alpha)}$, $\tau_s^{(\alpha)}$,$\dot{\gamma}_0{}^{(\alpha)}$) should be identified for each family of slip systems.
To keep the inverse identification problem more tractable, we assumed the same reference shear strain rate on each slip system α $\left(\dot{\gamma}_0{}^{(\alpha)} = \dot{\gamma}_0 = 1.0\ 10^{-3}\right)$ and strain rate sensitivity exponent $(n = 45)$.
Furthermore, the basal glide being the easy slip system for zinc, we assumed a constant ratio between basal and prismatic glide initial yield stresses $\left(\tau_0^{Prism}/\tau_0^{Basal} = 15\right)$, and between basal and pyramidal glide initial yield stresses $\left(\tau_0^{\pi\langle c+a\rangle}/\tau_0^{Basal} = 10\right)$, as suggested by Philippe *et al.* [20] and Fundenberger *et al.* [21]. Finally, the number of material parameters to identify is reduced to 7 ($h_0^{Basal}, h_0^{Prism}, h_0^{\pi\langle c+a\rangle}, \tau_0^{Basal}, \tau_s^{Basal}, \tau_s^{Prism}, \tau_s^{\pi<c+a>}$).
Those material parameters are obtained using an inverse identification procedure, by iteratively adjusting FE simulation and experimental load-penetration depth curves. The genetic algorithm MOGA-II to minimize the objective function defined as:

$$F_{obj} = \frac{1}{N}\sum_{i=1}^{N}\left(h_{\mathrm{num}}(\mathrm{P},\mathrm{t}_i) - h_{\exp}(t_i)\right)^2 \tag{5}$$

where *P* stands for the vector of unknown parameters, *N* is the number of data set, t_i denotes the time of the corresponding experimental point i, and $h_{num}(P,t_i)$ and $h_{exp}(t_i)$ are the indenter displacements numerically computed and experimentally measured, respectively.

5. Results and discussion

5.1. Identification of the crystal plasticity model parameters

To estimate the effect of cold rolling on the nanoindentation response of pure zinc grains, we have selected Grain #17 (AR: as-received annealed cold-rolled) and Grain #1 (TR: thickness reduction rate of 50%) for the identification of the crystal plasticity model parameters.
The identified parameters are summarized in table 3. It is found that increased percentage of cold reduction increases the critical resolved shear stresses (CRSS) $\tau_0^{(\alpha)}$. The main reasons for CRSS reduction are work hardening and grain refinement due to thickness reduction. Figure 3 depicts the experimental and numerical load-penetration depth curves issued from the identification procedure for the two selected grains. A good agreement between the experimental data and the FE simulation results can be observed for both selected grains. Moreover, the penetration depth at same load (1000 μN) is lower for Grain #1 with thickness reduction rate of 50% which is in accordance with the increase of the critical resolved shear stresses. Figure 4 shows the activity of slip systems in the area underneath the indenter. The basal and pyramidal systems are the more active systems. Basal system is the more active system for Grain #17 (figure 4a), while pyramidal system is more active for Grain #1 (figure 4c).

Table 3. Crystal plasticity model parameters identified.

Grain number - state	h_0^{Basal} (MPa)	h_0^{Pris} (MPa)	$h_0^{\pi\langle c+a\rangle}$ (MPa)	τ_0^{Basal} (MPa)	τ_s^{Basal} (MPa)	τ_s^{Pris} (MPa)	$\tau_s^{\pi<c+a>}$ (MPa)
1 - TR	214	635	1065	4.3	236	230	44
17 - AR	146	994	1364	3.49	284.5	136	43

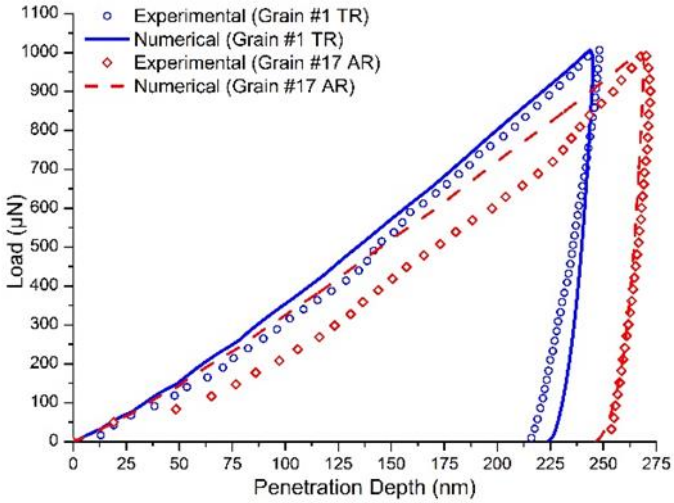

Figure 3. Experimental and simulated load-penetration depth curves.

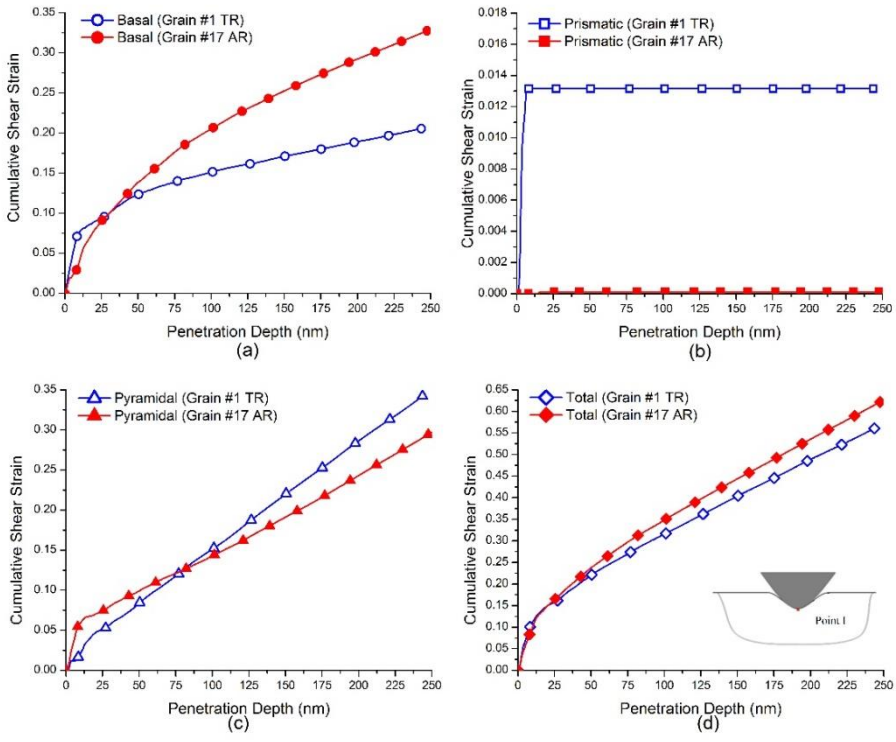

Figure 4. Evolution of $\gamma^{(\alpha)}$ in the area underneath the indenter.

5.2. Validation of the crystal plasticity model

To verify the validity of the proposed model, indentation tests performed on grains of different crystalline orientations were simulated using the CPFEM model with the identified parameters given in table 3. Grain #15 (AR: as-received annealed cold-rolled) and Grain #15 (TR: thickness reduction rate of 50%) were selected given their quite distinct location in the standard stereographic triangle, involving thus different slip systems activity rates.

The comparison between experimental data and numerical simulations is showed in figure 5. It is worth noting that the simulation results for both grains are in good agreement with the experimental data. Those results validate the identified model for a wide range of orientations.

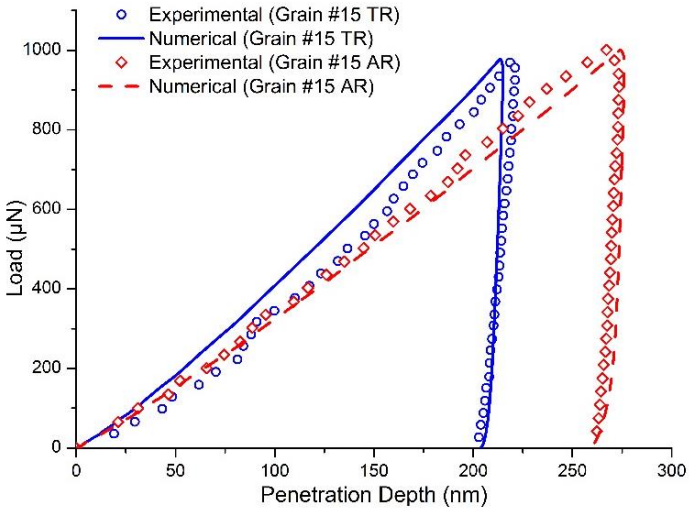

Figure 5. Experimental and simulated load-penetration depth curves.

6. Conclusion

In this work, we studied the orientation-dependent response of pure zinc grains subjected to two cold-rolling conditions. Instrumented indentation experiments were performed on grains of different crystalline orientations for as-received annealed cold-rolled material and material with thickness reduction rate of 50%. A crystal plasticity model was implemented in the FE code Abaqus using a user subroutine UMAT. The model parameters for both materials were identified by solving an inverse problem. It was found that increased percentage of cold reduction increases the critical resolved shear stresses (CRSS). Experimental data and numerical results are in good agreement for a wide range of orientations.

7. References

[1] H Takuda, T Yoshii and N Hatta 1999 *J. Mater. Process. Techn.* **89–90** p 135-140.
[2] T Kuwabara, C Katami, M Kikuchi, T Shindo and T Ohwue 2001 *In: Proceedings of the Seventh International Conference on Numerical Methods in Industrial Forming Processes, Toyohashi, Japan, 18-20 June,* p 781
[3] O Cazacu and F Barlat 2004 *Int. J Plast.* **20** p 2027-2045
[4] O Cazacu, B Plunkett and F Barlat 2006 *Int. J. Plast.* **22** p 1171-1194
[5] B Plunkett, R A Lebensohn, O Cazacu and F Barlat 2006 *Acta Mater.* **54** p 4159-4169
[6] M E Nixon, O Cazacu and R A Lebensohn 2010 *Int. J. Plast.* **26** p 516-532
[7] S K Khan, S Yu and H Liu 2012 *Int. J. Plast.* **38** p 14-26
[8] J H Yoon, O Cazacu and R K Mishra 2014 *Mater. Sci. Eng. A* **565** p 203-212

[9] C Zambaldi, Y Yang, T R Bieler and D Raabe 2012 *Journal of Materials Research* **27** p 356-367
[10] L Cauvin, B Raghavan, S Bouvier, X Wang and F Meraghni 2018 *Mater. Sci. Eng. A* **729** p 106-118
[11] N P T Nguyen, F Abbès, B Abbès and Y Li 2018 *H Nguyen-Xuan et al. (eds.), Proceedings of the International Conference on Advances in Computational Mechanics 2007, Lecture Notes in Mechanical Engineering* p 157-169
[12] D Peirce, R J Asaro and A Needleman 1983 *Acta Metall.* **31** p 1951-1976
[13] G I Taylor 1938 *J. Inst. Metals* **62** p 307-324
[14] M H Yoo and C T Wei 1966 *Philosophical Magazine* **13** p 759-775
[15] M H Yoo and J K Lee 1991 *Philosophical Magazine* **63** p 987-1000
[16] Y Huang 1991 *Mech Report 178* (Harvard University)
[17] J W Kysar and P Hall 1997 (Harvard University)
[18] Y Liu, B Wang, M Yoshino, S Roy, H Lu and R Komanduri 2005 *Journal of the Mechanics and Physics of Solids* **53** p 2718–2741
[19] Y Liu, S Varghese, J Ma, M Yoshino, H Lu and R Komanduri 2008 *International Journal of Plasticity* **24** p 1990–2015
[20] M J Philippe, M Serghat, P V Houtte and C Esling 1994 *Acta Metallurgica & Materalia* **42** p 239-250
[21] J J Fundenberger, M J Philippe, F Wagner and C Esling 1997 *Acta Materialia* **45** p 4041-4055